Geophys. J. Int. (2006) **165,** 943–956 doi: 10.1111/j.1365-246X.2006.02966.x

Non-linear seismic wave propagation in anisotropic media using the flux-corrected transport technique

Haishan Zheng,[1] Zhongjie Zhang[1] and Enru Liu[2]

[1]*Key Laboratory of Lithosphere Evolution, Institute of Geology and Geophysics, Chinese Academy of Sciences, Beijing* 100029, *China*
[2]*British Geological Survey, Murchison House, West Mains Road, Edinburgh* EH9 3LA, *UK. E-mail: E.Liu@bgs.ac.uk*

Accepted 2006 February 22. Received 2006 February 21; in original form 2005 April 14

SUMMARY

Both anisotropy and non-linearity of rocks are important properties related to the elastic wave propagation in the Earth. However, in the literature, there has been a continuous increase in the interest of anisotropy, but very few studies of non-linearity are reported. In this paper, we aim to tackle this imbalance by examining propagation characteristics of non-linear elastic waves in anisotropic media. As analytic solutions to anisotropic wave equation in non-linear media (or non-linear wave equation in anisotropic media) are not readily available, we use a numerical-based approach. However, we realize that numerical modelling of non-linear seismic waves suffers from problems such as steep gradients, shocks and unphysical oscillations. Accordingly, some special treatments have been presented in the literature to reduce these problems. In this paper, we present a second-order central finite difference scheme based on the modified flux-corrected transport (FCT) technique, and we also present the stability criterion for the FCT. Our modelling results show that the product of strength of non-linearity and the initial amplitudes of the seismic source is the main factor influencing propagation characteristics accumulated with traveltimes. Moreover, the effects of non-linear elastic wave propagation can be distorted by the initial frequency of the seismic source and become enhanced by the presence of anisotropy. Similarly, the effects induced by anisotropy are enhanced in non-linear media. Both in isotropic and vertical symmetry axis media, the non-linear effects, such as the waveform aberration (or waveform distortion), the resonant peak shift and the generation of harmonics, can be clearly seen, and the interaction between anisotropy and non-linearity is also obvious. In conclusion, both the anisotropy and the non-linearity should be considered to investigate characteristics of elastic wave propagation in solid media, especially when the source is strong (e.g. in source regions).

Key words: anisotropy, flux-corrected transport technique,non-linearity, wave propagation.

1 INTRODUCTION

The assumption that rocks are perfectly linearly elastic media is just a matter of simplicity, but it is not based on laboratory and field observations (Helbig & Rasolofosaon 2000). In fact, it is now well established that most rocks are anisotropic (their elastic response depends on directions of observations) and rocks exhibit a non-linear elastic response, which manifests itself in a variety of interrelated manners. That is, rocks are examples of consolidated materials whose primary physical properties are a consequence of the process of their genesis (Guyer & Johnson 1999).

Non-linear effects in rocks, such as non-linear dependence of seismic velocities on stress (Birch 1961), resonant peak shift (Winkler *et al.* 1979) and harmonic generation (Johnson *et al.* 1987) have been widely observed in laboratory experiments (Toksöz *et al.* 1976; Johnson & Shankland 1989) and studied since at least the later 1960s (Nikolaev 1967; Vasil'ev *et al.* 1969, 1977). Actually, non-linear elasticity in rocks influences many areas of Earth sciences, especially seismology, when the spectral distortion of seismic waves is considered (Bulau *et al.* 1984). Many experiments with crystalline rocks have shown a strong non-linear elastic response (Johnson *et al.* 1987), and accordingly the third-order elastic tensors have been given in the literature (Prosser & Green 1990; Prosser *et al.* 1992). Another well-known fact is the presence of anisotropy in almost all rock types (Crampin 1987). For example, many sedimentary rocks contain fine layering or aligned cracks, joints and fractures, giving rise to seismic anisotropy. Fracture orientations, current stress fields, and preferred fluid-flow direction in hydrocarbon reservoirs may be effectively predicted using the concept of seismic anisotropy. The significance of the seismic anisotropy in exploration geophysics is well summarized by Helbig (1994), Liu *et al.* (2000) and Lynn (1996), and in global seismology by Savage (1999).

© 2006 The Authors
Journal compilation © 2006 RAS

As both non-linearity and anisotropy in rocks are believed to be important aspects for the propagation of elastic waves in the Earth, the following problems should be properly addressed: (a) differentiation of linear and non-linear elastic waves; (b) which of the two aspects are more important for elastic wave propagation and (c) the characterisation of non-linear elastic waves in anisotropic media. In this paper, we provide some answers, to these questions through numerical modelling of non-linear elastic waves in anisotropic (vertical symmetry axis; VTI) media. Note that it may be argued that the three problems mentioned here are only meaningful in theory as in practice all rocks are anisotropic and non-linear, and only when anisotropy or non-linearity is weak, can we differentiate anisotropy and non-linearity. While this argument may be correct for weak anisotropy, non-linearity may be resolved, and similarly for non-linearity, anisotropy may be characterized. We aim to draw the attention to this subject as we feel that some of the effects due to non-linearity (e.g. waveform distortion, peak frequency shifts) may easily be mistaken as due to dispersion or attenuation.

Non-linear elastic wave equations in rocks (with anisotropic characteristics) have been presented in several papers (Murnaghan 1951; Landau & Lifshitz 1986; Xu *et al.* 1999). Unfortunately, it is difficult to obtain analytic solutions in these cases. A representative analytic method is the iterative technique based on Green's function developed by McCall (1994) and McCall & Guyer (1994). In this method, the solution of the 1-D non-linear wave equation is represented as a power series. However, closed-form solutions can only be obtained for a few special cases. Consequently, it is necessary to use numerical methods, such as explicit or implicit finite difference (FD) schemes, pseudospectral methods on standard or staggered grids, finite elements or spectral element methods (Levander 1988; Frankel & Leith 1992; Schultz 1997; Komatitsch & Tromp 1999; Zhang *et al.* 1993, 1999). However, numerical methods have some difficulties to address problems like steep gradients, unphysical numerical oscillations and shocks related to the propagation of non-linear waves in anisotropic media. To avoid or reduce these problems, special treatments have to be adapted in the numerical modelling of non-linear waves. For examples, Scalerandi *et al.* (1999) used two FD schemes with different orders of accuracy in both space and time to investigate non-linear acoustic waves; Zheng *et al.* (2004) used this method to study non-linear elastic waves in media where elastic properties vary in 1-D; Kouri *et al.* (1999) obtained numerical solutions of non-linear wave equations by setting limits to the maximum value of the displacement. Daniel (1997) obtained numerical solutions of a non-linear wave equation derived from the FPU model (after Fermi *et al.* 1974; Ulam 1965, 1974) by setting limits to the maximum values of the spatial derivatives of displacements.

These studies resulted in many interesting and significant results for the non-linear elastic waves, although the problems of steep gradients and shocks are still very severe. At the same time, the unphysical oscillations caused by the discretization of the wave equation and the error accumulation could not be completely eliminated. To overcome the undesirable ripples in wavefield simulations, Boris & Book (1973, 1976a,b) and Book *et al.* (1975) developed a flux-corrected transport (FCT) technique to solve the first-order system of continuity equations in hydrodynamics (DeVore 1991). Fei & Larner (1995) and Yang *et al.* (2002) have applied the FCT technique to the second-order partial differential equations in order to improve the accuracy of numerical solutions. However, this method cannot be used directly to solve the problems of non-linear wave propagation, especially when the non-linearity is strong or the displacements are large.

We presented a modified FCT technique consisting of an additional correction stage added to the FCT algorithm reported by Yang *et al.* (2002). The technique is very effective to overcome the problems mentioned before, and it does not destroy the characteristics of non-linear waves.

In this paper, we firstly deduce the non-linear elastic wave equation for displacements u_x and u_z in 2-D transversely isotropic media with a VTI. We then present in detail the modified FCT technique based on second-order central FDs scheme (hereafter referred to as MFCT) and the stability criterion. This method is numerically tested using several examples to show various non-linear and anisotropic effects. We also investigate the spectral characteristics of linear and non-linear wave propagation and compare the time-series (waveforms) of linear and non-linear elastic waves propagating in isotropic and anisotropic media. Our main aim is to draw attentions to the different effects caused by non-linearity and anisotropy, and with the loss of generality, we only consider the most commonly used, yet simplest, anisotropic media, that is, transversely isotropic media with a VTI. Other type of anisotropy may be studied in a similar way using the method presented in this paper, but our general conclusions are expected to also hold essentially for more general anisotropy.

2 NON-LINEAR ELASTIC WAVE EQUATION AND FINITE-DIFFERENCE SCHEME

The non-linear elastic wave equation is given by Murnaghan (1951), Engelbrecht (1983) and Landau & Lifshitz (1986). Here we use the general equation presented by Rasolofosaon & Yin (1996):

$$\rho\ddot{u}_i = \frac{\partial^2}{\partial x_j \partial x_l}\left[C_{ijkl} + \left(C^{(\text{NLphysical})}_{ijklmn} + C^{(\text{NLgeometrical})}_{ijklmn}\right)\frac{\partial u_m}{\partial x_n}\right]u_k, \tag{1}$$

where

$$C^{(\text{NLphysical})}_{ijklmn} = C_{ijklmn},$$

and

$$C^{(\text{NLgeometrical})}_{ijklmn} = C_{ijlm}\delta_{kn} + C_{ilnm}\delta_{jk} + C_{iklm}\delta_{jn},$$

where ρ designates density, t is the time, x_j is the jth component of position vector, u_i is the ith component of displacements, C_{ijkl} and C_{ijklmn} (i, j, k, l, m, n = 1, 2, 3) are the components of the fourth-rank or second-order elastic (SOE) tensor and the sixth-rank or third-order elastic (TOE) tensor, respectively, and δ is the Kronecker symbol. There are two types of non-linearity represented in eq. (1), one is $C^{(\text{NLgeometrical})}_{ijklmn}$,

called geometrical non-linearity, which accounts for the non-linear relationship between strain and displacement when finite deformations are taken into account. The other type of non-linearity, $C_{ijklmn}^{(\mathrm{NLphysical})}$, is 'physical', which is contained in the TOE coefficients. We can condense a pair of indices (i, j) into a single index I following the rule of the standard Voigt notation, that is,$11 \rightarrow 1$, $22 \rightarrow 2$, $33 \rightarrow 3$, $23 \rightarrow 4$, $13 \rightarrow 5$, and $12 \rightarrow 6$. For example, C_{3312} and C_{113313} can be simply replaced by C_{36} and C_{135}, respectively. In VTI media, the independent components of C_{ijkl} and C_{ijklmn} are C_{11}, C_{12}, C_{13}, C_{33}, C_{44} and C_{111}, C_{112}, C_{113}, C_{123}, C_{133}, C_{144}, C_{155}, C_{222}, C_{333} and C_{344}, respectively (Hermon 1953). Helbig (1998, 2000) has given a comprehensive analysis of the properties of these two tensors including some clarifications of terminology used in the literature.

Substituting these independent components and the corresponding non-zero components of the SOE and TOE constants into eq. (1), and considering in 2-D media the components u_x and u_z, we can obtain the non-linear elastic wave equation in VTI media,

$$\rho(x,z)\frac{\partial^2 \mathbf{U}}{\partial t^2} = \frac{\partial}{\partial x}\left(\mathbf{A}\frac{\partial}{\partial x} + \mathbf{D}\frac{\partial}{\partial z}\right)\mathbf{U} + \frac{\partial}{\partial z}\left(\mathbf{G}\frac{\partial}{\partial x} + \mathbf{Q}\frac{\partial}{\partial z}\right)\mathbf{U} + \mathbf{F}, \tag{2}$$

where

$$\mathbf{A} = \begin{bmatrix} C_{11} + (C_{111} + 3C_{11})\frac{\partial u_x}{\partial x} + (C_{113} + C_{13})\frac{\partial u_z}{\partial z} & (C_{155} + C_{55})\frac{\partial u_z}{\partial x} + (C_{155} + C_{11})\frac{\partial u_x}{\partial z} \\ (C_{155} + 3C_{55})\frac{\partial u_z}{\partial x} + (C_{155} + C_{55})\frac{\partial u_x}{\partial z} & C_{55} + (C_{155} + C_{13})\frac{\partial u_x}{\partial x} + (C_{355} + C_{55})\frac{\partial u_z}{\partial z}, \end{bmatrix}$$

$$\mathbf{D} = \begin{bmatrix} (C_{155} + C_{55} + 2C_{13})\frac{\partial u_z}{\partial x} + (C_{155} + C_{55})\frac{\partial u_x}{\partial z} & C_{13} + (C_{113} + C_{55})\frac{\partial u_x}{\partial x} + (C_{133} + C_{13})\frac{\partial u_z}{\partial z} \\ C_{55} + (C_{155} + 2C_{55} + C_{13})\frac{\partial u_x}{\partial x} + (C_{33} + C_{355})\frac{\partial u_z}{\partial z} & (C_{355} + C_{33})\frac{\partial u_z}{\partial x} + (C_{355} + C_{55})\frac{\partial u_x}{\partial z} \end{bmatrix}$$

$$\mathbf{G} = \begin{bmatrix} (C_{155} + C_{55})\frac{\partial u_z}{\partial x} + (C_{155} + C_{11})\frac{\partial u_x}{\partial z} & C_{55} + (C_{155} + C_{11})\frac{\partial u_x}{\partial x} + (C_{355} + C_{13} + 2C_{55})\frac{\partial u_z}{\partial z} \\ C_{13} + (C_{113} + C_{13})\frac{\partial u_x}{\partial x} + (C_{133} + C_{55})\frac{\partial u_z}{\partial z} & (C_{355} + C_{55})\frac{\partial u_z}{\partial x} + (C_{355} + C_{55} + 2C_{13})\frac{\partial u_x}{\partial z} \end{bmatrix}$$

$$\mathbf{Q} = \begin{bmatrix} C_{55} + (C_{155} + C_{55})\frac{\partial u_x}{\partial x} + (C_{355} + C_{13})\frac{\partial u_z}{\partial z} & (C_{355} + C_{55})\frac{\partial u_z}{\partial x} + (C_{355} + 3C_{55})\frac{\partial u_x}{\partial z} \\ (C_{355} + C_{33})\frac{\partial u_z}{\partial x} + (C_{355} + C_{55})\frac{\partial u_x}{\partial z} & C_{33} + (C_{133} + C_{13})\frac{\partial u_x}{\partial x} + (C_{333} + 3C_{33})\frac{\partial u_z}{\partial z}, \end{bmatrix}$$

where $\mathbf{U} = (u_x, u_z)^T$, $\mathbf{F} = (f_x, f_z)^T$ and f_x, f_z denote the components of the source in x- and z-directions. Using the central difference scheme to approximate eq. (2) without the source term $\mathbf{F}$, we have

$$\begin{aligned} U_{i,j}^{n+1} = {} & 2U_{i,j}^{n} - U_{i,j}^{n-1} + m^2 A_{i,j}\left(U_{i+1,j}^{n} - 2U_{i,j}^{n} + U_{i-1,j}^{n}\right)/\rho_{i,j} \\ & + n^2 A_{i,j}\left(U_{i+1,j}^{n} - 2U_{i,j}^{n} + U_{i-1,j}^{n}\right)/\rho_{i,j} \\ & + l^2 (D_{i,j} + G_{i,j})\left(U_{i+1,j+1}^{n} + U_{i-1,j-1}^{n} - U_{i+1,j-1}^{n} - U_{i-1,j+1}^{n}\right)/\rho_{i,j}, \end{aligned} \tag{3}$$

where $m = \Delta t/\Delta x$, $n = \Delta t/\Delta z$, $l = \Delta t/2\sqrt{\Delta x \Delta z}$, Δx and Δz being the spatial increments in x- and z-directions, respectively; Δt is the time-step size, and $U^n{}_{i,j} = U(i\Delta x, j\Delta z, n\Delta t)$. Similarly, we can apply the discrete scheme to replace $\partial \mathbf{U}/\partial x$ and $\partial \mathbf{U}/\partial z$ in the matrices $\mathbf{A}$, $\mathbf{D}$, $\mathbf{G}$ and $\mathbf{Q}$ by $(U^n{}_{i+1,j} - U^n{}_{i-1,j})/(2\Delta x)$ and $(U^n{}_{i,j+1} - U^n{}_{i,j-1})/(2\Delta z)$.

According to the analyses similar to those presented by Richtmyer & Morton (1967) and Yang *et al.* (2002), and through a series of mathematical operations, we can obtain the stability criterion for the FD scheme in eq. (3) (see details in Appendix A).

3 THE MODIFIED FCT FINITE-DIFFERENCE ALGORITHM

The numerical modelling of non-linear seismic waves suffers from several problems such as the steep gradients, shocks and unphysical oscillations and, therefore, the numerical computation may become unstable. To reduce these drawbacks, some special treatments have been proposed. A typical procedure is given by Kouri *et al.* (1999), in which the displacement is constrained by $u < u_{\max}$. Another typical procedure is suggested by Daniel (1997), in which the value of local $\partial u_i/\partial x_j$ is constrained similarly. However, in the first method, the selection of proper limit $u_{\max}$ is difficult: if $u_{\max}$ is too large, it will be useless to reduce above drawbacks, if it is too small, it will severely decrease the numerical accuracy. As for the second method, u_i has to be used to calculate $\partial u_i/\partial x_j$ before the correction procedure. After the correction, $\partial u_i/\partial x_j$ will be used to calculate u_i. Obviously, these processes will introduce new errors to the numerical solutions and make the numerical modelling more difficult.

Fortunately, the FCT technique originally presented by Boris & Book (1973, 1976a,b) and Book *et al.* (1975), and later extended by Yang *et al.* (2002), can be used to tackle some of these problems, since it can not only remove the problems caused by the modelling of non-linear waves, but also maintain the characteristics of non-linear waves. Following Yang *et al.* (2002), the FCT-based FD algorithm consists of three stages: FDs for solving eq. (3); diffusion computation, and offsetting diffusion. However, the validity of the FCT technique is uncertain when the value of the displacement u_i, obtained by numerical calculation is too large in some local zones. As a consequence, we propose to modify the FCT technique to include an additional stage, in which a limiting function for the solutions is used to correct u_i. We shall call this modified FCT as MFCT (see details in Appendix B).

© 2006 The Authors, *GJI*, **165,** 943–956
Journal compilation © 2006 RAS

4 NUMERICAL EXPERIMENTS

We put the seismic source with equivalent energy of shear and compressional waves at the centre of the study domain. The source function is a Ricker wavelet,

$$S(t) = S_A[1 - (2\pi ft)^2/2]\exp[-(2\pi ft)^2], \tag{4}$$

which has to be convolved with the source term **F** in eq. (2) during numerical computation to obtain displacements. In this paper, we take the source strength $Sa = 0.003$ (in unit force), peak frequency $f = 30$ Hz. In the FD calculations, the time interval $\Delta t = 0.2$ ms, and spatial grid intervals $\Delta x = \Delta z = 5$ m. Note that we vary the value of Sa to give an indication of the source strength (the absolute value of Sa is only used as a reference, and the relative value between various plots involving variations of Sa is more meaningful. For plotting purpose, we use small values of Sa in order to achieve some sensible values for displacements u_x and u_x). To record the forward propagating waves only, a moving boundary around the seismic source is set during the computation. Johnson & Rasolofosaon (1996) suggested that the magnitude of the non-linearity is quantified by the ratio between the TOE and the SOE constants. We introduce three global non-linearity parameters,

$$SN_p = \frac{\|\tilde{C}^{\text{NLphysical}}\|}{\|\tilde{C}^{\text{Linear}}\|}, \tag{5a}$$

$$SN_g = \frac{\|\tilde{C}^{\text{NLgeometrical}}\|}{\|\tilde{C}^{\text{Linear}}\|}, \tag{5b}$$

$$SN = SN_g + SN_p, \tag{5c}$$

where $\|\cdot\|$ denotes the norm of a tensor, $\tilde{C}^{\text{Linear}}$, $\tilde{C}^{\text{NLphysical}}$ and $\tilde{C}^{\text{NLgeometrical}}$ denote the linear elastic tensor, the physical non-linear elastic tensor and the geometrical non-linear elastic tensor, respectively. SNp and SN_g can be compared to determine whether the geometrical or physical non-linearity dominates the non-linear elastic phenomena in a given material. SN denotes the total non-linear strength. The explicit expressions of $\tilde{C}^{\text{Linear}}$, $\tilde{C}^{\text{NLphysical}}$and $\tilde{C}^{\text{NLgeometrical}}$ are given in Appendix C. Note that the use of eq. (5) to quantify the magnitude of non-linearity is not strictly valid. The reason is that though the second-order and third-order tensors have the same dimension (in Pa), one cannot compare tensors of different ranks. The difficulty is caused by the fact that in Hooke's law the two tensors are multiplied, respectively, with ε_{ij} and $\varepsilon_{ij}\,\varepsilon_{mn}$ and the strain tensor $\boldsymbol{\varepsilon}$ is formally dimensionless. Ideally we would prefer a dimensionless number that allows us to compare different materials and the proper (and valid) way would be to compare the C_{ijkl} with $\varepsilon_{mn}\,C_{ijklmn}$. Helbig (1998, 2000) has discussed this problem in great details, who suggests to use eigenstrains and eigenstiffnesses using Kelvin notation of elastic tensors.

To show the different effects caused by anisotropy and non-linearity, we introduce two variables,

$$X_{u-v}(t) = X_{u-v}(n\Delta t) = \frac{\sum_{i,j} abs\left(u^n_{i,j} - v^n_{i,j}\right)}{\sum_{i,j} abs\left(v^n_{i,j}\right)}, \tag{6a}$$

$$Y_{u-v}(t) = Y_{u-v}(n\Delta t) = \frac{\sum_{i,j} abs\left(u^n_{i,j}\right) - abs\left(v^n_{i,j}\right)}{\sum_{i,j} abs\left(v^n_{i,j}\right)}, \tag{6b}$$

where $u^n{}_{i,j}$ and $v^n{}_{i,j}$ denote model displacements at the location (i, j) when $t = n\Delta t$ for elastic waves propagating in two different kinds of media, in which the displacements are denoted by u and v, respectively. The summation in eq. (6) is over number of samples on windowed traces. The eq. (6) will be used to quantify the effects of anisotropy and non-linearity on recorded seismic traces. Their physical meaning will be explained in Section 4.2.

The solid media are represented by the respective SOE and TOE constants. In the following numerical examples, the following values for the SOE and TOE coefficients are used as a reference. For the isotropic medium, we choose $C_{11} = C_{33} = 28.5$ GPa, $C_{13} = C_{55} = 9.5$ GPa, $C_{111} = C_{333} = -780$ GPa, $C_{113} = C_{133} = -180$ GPa, $C_{155} = C_{355} = -150$ GPa, and we simply call this material BMIN and obtain $SN_g = 9.25$, $SNp = 54.7$ and $SN = 63.99$. For the VTI medium, $C_{11} = 28.5$ GPa, $C_{33} = 30$ GPa, $C_{13} = 6$ GPa, $C_{55} = 9.5$ Gpa, $C_{111} = -780$ GPa, $C_{333} = -850$ GPa, $C_{113} = -16$ GPa, $C_{133} = -90$ GPa, $C_{155} = -108$ GPa, $C_{355} = -154$ GPa, and we simply call this material BMAIN and obtain $SN_g = 9.14$, $SNp = 50.26$ and $SN = 59.40$. An average value of density $\rho = 2.75$ g cm $^{-3}$ is used for all the examples. In our examples in the next section, we shall vary the values of SN_g, SNp and SN so to cover the expected strain levels near source regions.

4.1 MFCT–FD algorithm versus FD

First of all, two facts must be mentioned in order to emphasize the efficiency of the MFCT–FD algorithm. The first fact is that the MFCT–FD algorithm does not induce additional distortions to the waveforms, which can be substantiated by comparing the numerical solutions reported by standard FD and MFCT–FD for linear waves. The other fact is that the MFCT–FD algorithm is very efficient to reduce or even to eliminate the problems of steep gradients, shocks and unphysical oscillations generated by non-linear wave propagation, which can be seen by comparing the numerical solutions given by FD and MTCT-FD for non-linear waves. To show these two facts,

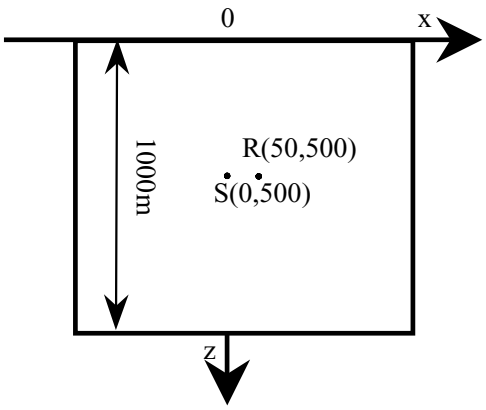

Figure 1. Model 1. Seismic source S (0, 500) ($x = 0$ m, $z = 500$ m) is located at the centre of an isotropic medium where $SNp = 54.74$, $SN = 63.99$, and a recording point R is set at $x = 50$ m, $z = 500$ m.

we consider a simple isotropic full-space (no layers) model with SOE constants as those of BMIN, model1 (the model geometry, source S and receiver R positions are shown in Fig. 1). The numerical results are shown in Fig. 2. We can see that the MFCT–FD algorithm is effective to overcome problems from the numerical modelling of non-linear elastic waves without large distortions of the waveforms. The undesirable oscillation trails appear in the results of the conventional FD method when the non-linearity or source energy becomes stronger.

4.2 Anisotropic and non-linear effects

In the following we use the notations, X_{im-n} and Y_{im-n}, $i = x$ or $i = z$, for displacements u_x, v_x, or u_z, v_z, respectively, in eqs (6a) and (6b); Indices m and n denote the type of models used. Four models are used here, namely, linear elastic waves propagating in isotropic media, which are denoted as 'IL'; linear elastic waves propagating in anisotropic (VTI) media, denoted as 'AL'; non-linear elastic waves propagating in isotropic media, denoted as 'IN'; and non-linear elastic waves propagating in anisotropic (VTI) media, denoted as 'AN'. For example, X_{xAL-IL} represents the x- component calculated by linear elastic wave displacement u_x in VTI media and linear elastic wave displacement v_x in isotropic media. X and Y represent the difference in amplitudes (the absolute value of the displacement) and phases (the sign of the displacement) between u and v corresponding to elastic waves in two kinds of media. Thus, they can be used to investigate the effect due to the presence of anisotropy or non-linearity.

To investigate the different effects caused by anisotropy and non-linearity, we calculate $x-$ and $y-$ component synthetic seismograms using the values given to the source strength S_A, the frequency f and the variable SN. Fig. 3 shows the results for X_{xAL-IL}, X_{zAL-IL}, Y_{xAL-IL} and Y_{zAL-IL} for three values of peak frequency f (Figs 3a–d) and two values of source strength S_A (Figs 3e–h). As for the plots for different frequency f, similar synthetic traces are obtained and only small difference among them can be observed. In particular, all of them reach constant values after seismic waves travel a certain distance. For example, Y_{xAL-IL} and Y_{zAL-IL} reach to 0.065 and 0.0735, respectively. Thus different frequencies f do not lead to different anisotropic effects. Similarly, from the plots computed for different values of the source strength S_A, we may conclude that the anisotropic effects do not depend on the energy of seismic source. (Note that what we have implied here is that anisotropy is a property of the medium concerned, and it does not vary with source strengths, frequency or source–medium distance. Obviously, we understand that anisotropy is always a consequence of internal structures, for example, caused by fabric, cracks and joints, and thus depends on the ration of wavelength to the characteristic scale-length, in which case both second-order and third-order tensors will be frequency/scale dependent, see for example Liu *et al.* 2003, for a discussion about frequency-dependent seismic anisotropy).

To show the non-linear effects more clearly, we increase the value of each TOE constant by a factor of 2, and thus $SN_g = 9.25, SN_p = 109.47$ and $SN = 118.72$. Varying the frequency f, we obtain the corresponding time-series of X_{xIN-IL}, X_{zIN-IL}, Y_{xIN-IL} and Y_{zIN-IL} shown in Figs 4(a)–(d). We find that there are three distinct stages in these plots: the rapid increase stage, from the initial time to 0.03 s; the steady change stage, from 0.03 to 0.13 s; the steady increase stage, after 0.13 s. Comparing with Fig. 3, we can see that the values of X are no longer significantly smaller than those of Y at the same time, but the variation of X is similar to that of Y in Fig. 4. These different features of X and Y between Figs 3 and 4 can be attributed to the different effects of anisotropy and non-linearity. Since no convergent values of X and Y are seen in Fig. 4, we can say that the non-linear effect may have some link with the peak frequency f of the seismic source function, which is expected so if the source function is expressed as displacement, and while strain varies with frequency. Keeping the same values of the TOE constants and varying the value of source S_A, we can obtain the time-series of X_{xIN-IL}, X_{zIN-IL}, Y_{xIN-IL} and Y_{zIN-IL} as shown in Figs 4(e)–(h). Obviously, the differences between the dotted lines and dashed lines are much smaller than those between the solid lines and dotted lines, and the slopes of solid lines both in the plots of X and Y after 0.13 s are almost three times larger than those presented in dotted lines and five times larger than those presented in dashed lines. Accordingly, we know that the non-linear effects that accumulate with traveltime following a non-linear function become more evident when the source strength S_A increases.

© 2006 The Authors, *GJI*, **165,** 943–956
Journal compilation © 2006 RAS

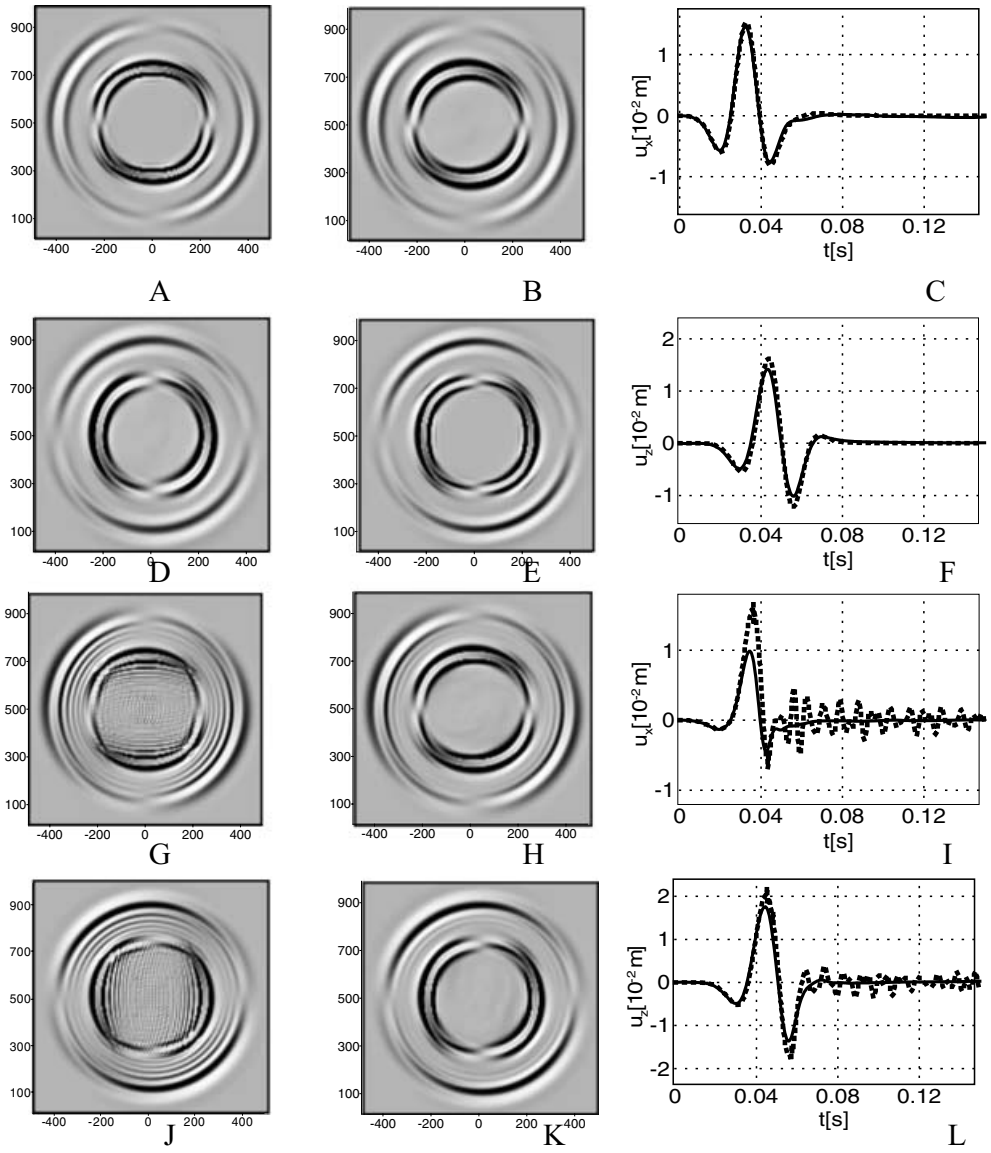

Figure 2. Snapshots and waveforms of linear and non-linear waves reported by FD (the first column and dotted lines in the third column) and MFCT–FD (the second column and solid lines in the third column) corresponding to model 1. The first and third row (A, B, C, G, H, J) figures correspond to u_x; The second and fourth row (D, E, F, J, K, L) figures correspond to u_z. The waveforms recorded at point R (Fig. 1) are shown in plots C, F, I and L.

In the subsequent examples, we only vary the values of each TOE constant and obtain the time-series of X_{xIN-IL}, X_{zIN-IL}, Y_{xIN-IL} and Y_{zIN-IL}. The results are shown in Fig. 5 for four kinds of non-linearity. We set each TOE constant equal to 2.5 times ($SN_g = 9.25, SNp = 136.84$ and $SN = 146.09$), twice ($SN_g = 9.25, SNp = 109.47$ and $SN = 118.7$), 1.2 times $SN_g = 9.25, SNp = 54.74$ and $SN = 63.99$) and 0.4 times ($SN_g = 9.25, SNp = 21.89$ and $SN = 31.14$) of that for BMIN. From Fig. 5, we can see that the effect of non-linearity in isotropic media depends on its strength. The plots of X_{xIN-IL}, X_{zIN-IL}, Y_{xIN-IL} and Y_{zIN-IL} shown in Fig. 5 have similar variations with traveltime as those shown in Fig. 4. Particularly, we can identify almost the same curves of X_{xIN-IL}, X_{zIN-IL}, Y_{xIN-IL} and Y_{zIN-IL} from Figs 4 and 5 when the product of SN and S_A has the same value. Therefore, we may conclude that the product of SN and S_A dominates the non-linear effect of elastic wave propagation.

Comparing the variations of Y in Figs 4 and 5 with those in Fig. 3, we see that the anisotropic effects have similar strengths as the non-linear effects when SA is less than 0.0005 (Fig. 4) or SN is less than about 31 (Fig. 5), that is, the product of S_A and SN is less than 0.06. We may also consider the case when the strengths of anisotropy and the strength of non-linearity are similar. However, in this case, both the variations and absolute value of X are clearly different (see Figs 3–5) just because of the different features of linear elastic wave propagation in anisotropic (VTI) media and non-linear elastic wave propagating in isotropic media. Moreover, the strength of effects introduced by non-linearity is accumulated with time.

To compare and specify the characteristics of non-linear effects in anisotropic (VTI) media, four kinds of X and Y time-series in different media are computed (Fig. 6), i.e. X_{xAL-IL}, X_{zAL-IL}, Y_{xAL-IL} and Y_{zAL-IL} ; X_{xIN-IL}, X_{zIN-IL}, Y_{xIN-IL} and Y_{zIN-IL} (same as those in Fig. 5,

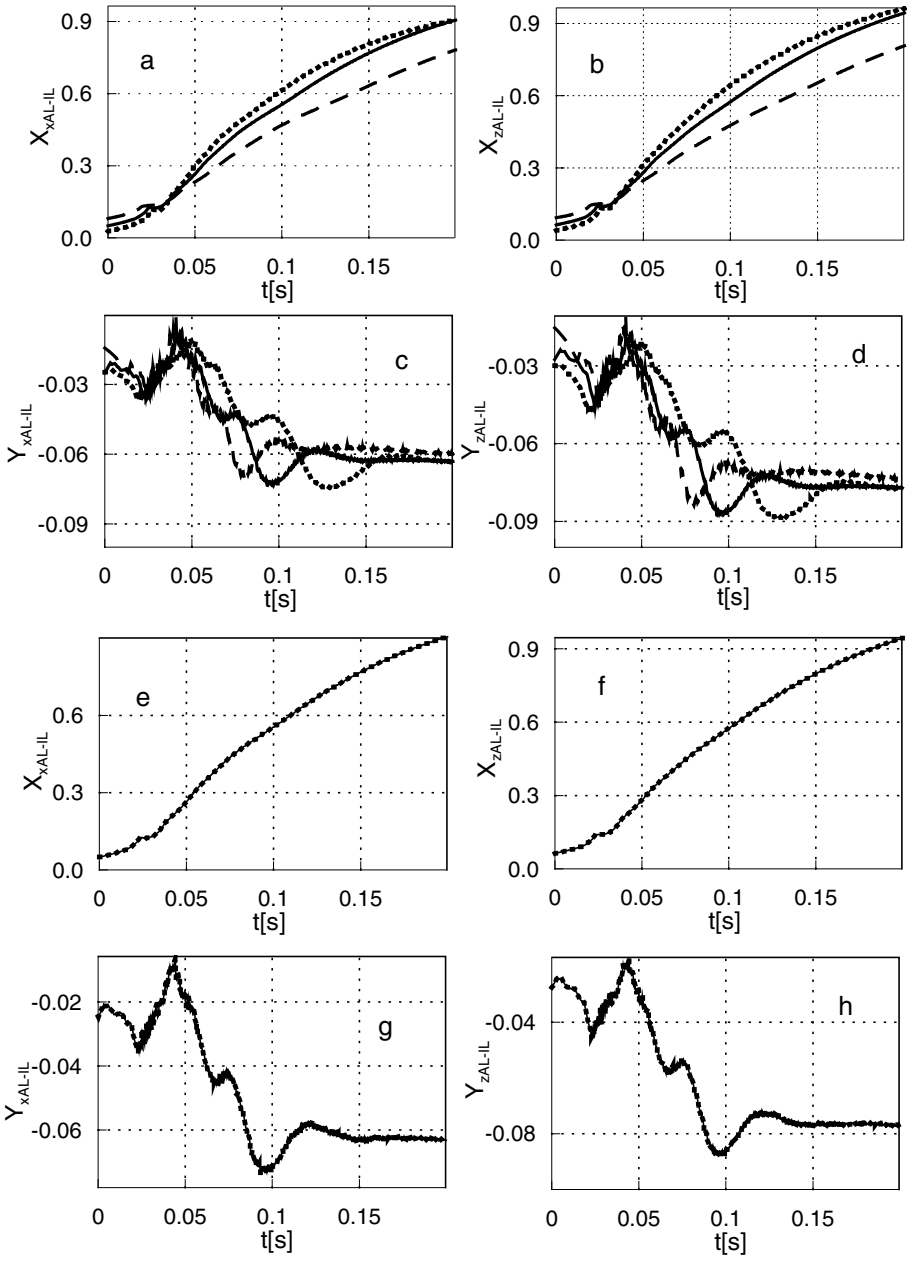

Figure 3. Time-series of X and Y calculated by linear elastic wave propagation in isotropic and anisotropic (VTI) media. Plots a, b, c, d correspond to different value of initial frequency f, namely, solid lines ($f = 30$ Hz), dashed lines ($f = 40$ Hz) and dotted lines ($f = 20$ Hz). Plots e, f, g, h correspond to different value of S_A, namely, solid lines ($S_A = 0.008$) and dotted lines ($S_A = 0.002$).

$SN = 118.72$); X_{xAN-IL}, X_{zAN-IL}, Y_{xAN-IL} and Y_{zAN-IL}($SN = 103$) and X_{xAN-AL}, X_{zAN-AL}, Y_{xAN-AL} and Y_{zAN-AL}($SN = 98.58$). We can see clearly the following two features of elastic waves in isotropic and VTI media. Firstly, comparing the solid lines with the dotted lines, we see the non-linear effect in VTI media is more evident than that in isotropic media when the strength of non-linearity in these two media is similar. The second feature is that the anisotropic effects in non-linear VTI media become enhanced and, therefore, clearer than those in linear VTI media.

4.3 Non-linear elastic waveforms

The non-linear waves exhibit distinct propagation characteristics, such as waveform distortion (Zheng *et al.* 2004), resonant peak shift (Winkler *et al.* 1979), or harmonic generation (Johnson *et al.* 1987). However, most of these results were obtained for acoustic waves or only one type of elastic waves propagating in isotropic media. To investigate the characteristics of non-linear elastic waves in both time and frequency domains, we consider the isotropic and VTI model shown in Fig. 7, where two receivers are located at different points.

The linear (solid lines) and non-linear (dashed lines) elastic waveforms recorded in isotropic medium at receiver $R1$ are shown in Fig. 8. We can see the waveform distortions in the time domain. Similarly, in the frequency domain, the resonant peak shift and harmonic generation corresponding to non-linear elastic waves are enhanced for the displacements u_x and u_z.

© 2006 The Authors, *GJI*, **165,** 943–956
Journal compilation © 2006 RAS

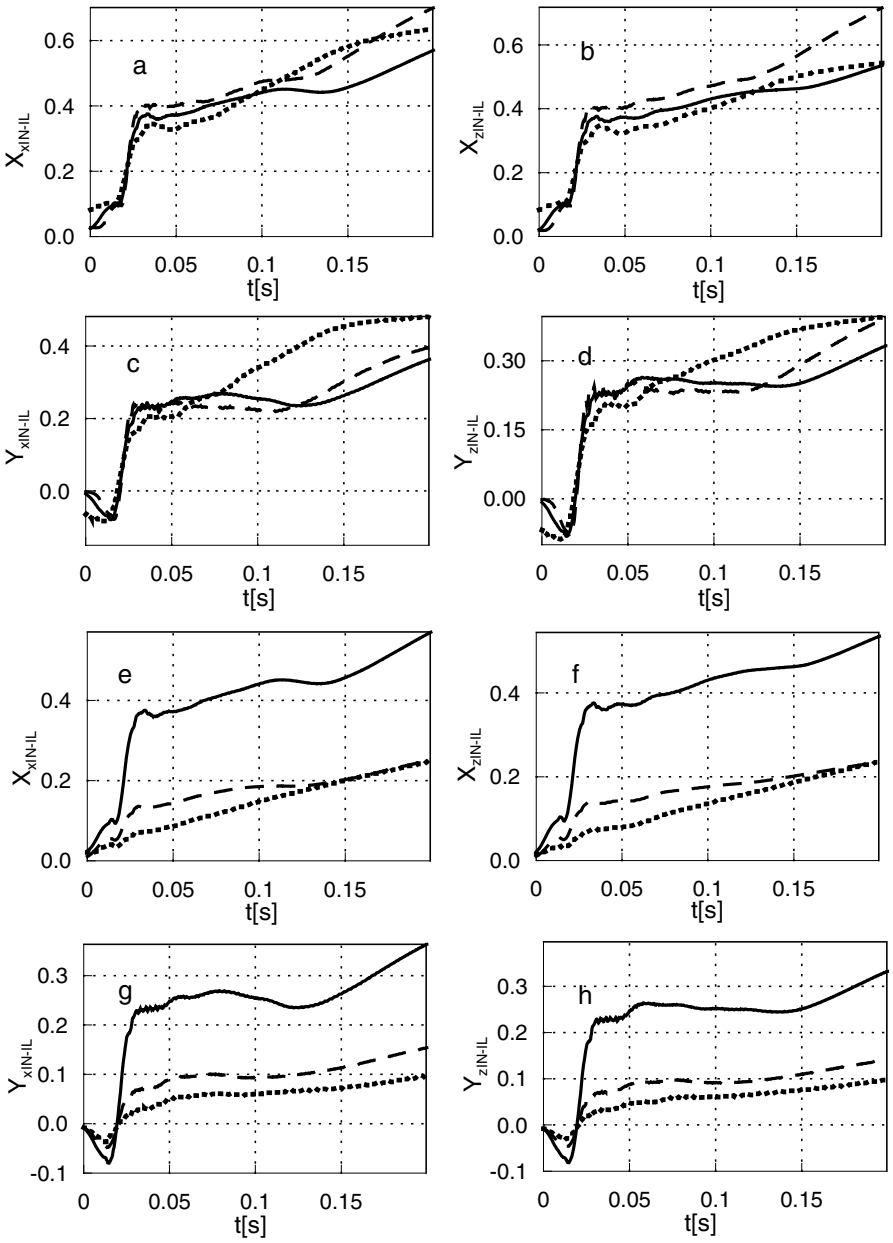

Figure 4. Time-series of X and Y calculated by non-linear and linear elastic wave propagation in isotropic. Plots a, b, c, d correspond to different value of initial frequency f, namely, solid lines ($f = 30$ Hz), dashed lines ($f = 40$ Hz) and dotted lines ($f = 20$ Hz). Plots e, f, g, h correspond to different value of S_A, namely, solid lines ($S_A = 0.002$), dashed lines ($S_A = 0.001$) and dotted lines ($S_A = 0.0005$).

The linear and non-linear elastic waveforms recorded in a VTI medium at receiver points $R1$ and $R2$ are given in Fig. 9, from which the distortions of non-linear elastic waveforms in the time domain are also clear. In the frequency domain, the resonant peak shift and harmonic generation corresponding to the non-linear elastic waves are also obvious in the both displacements u_x and u_z. In comparison with the propagation characteristics presented by the non-linear elastic waves propagating in the isotropic medium (Fig. 8), the non-linear elastic waves in VTI media become more complex, and in particular, they vary with directions (hence anisotropic).

5 DISCUSSION AND CONCLUSIONS

We have proposed a modified flux-corrected transport (MFCT)-based FD method to simultaneously take into account the effects of anisotropy and non-linearity in wave propagations. It is successfully used to avoid problems such as steep gradients, shocks and unphysical oscillations, which occur in the modelling of non-linear seismic waves with 'unmodified' methods, and to obtain stable and accurate numerical solutions to non-linear seismic wave equation. Based on the successful implementation of the MFCT algorithm, we may apply it to other FD schemes with

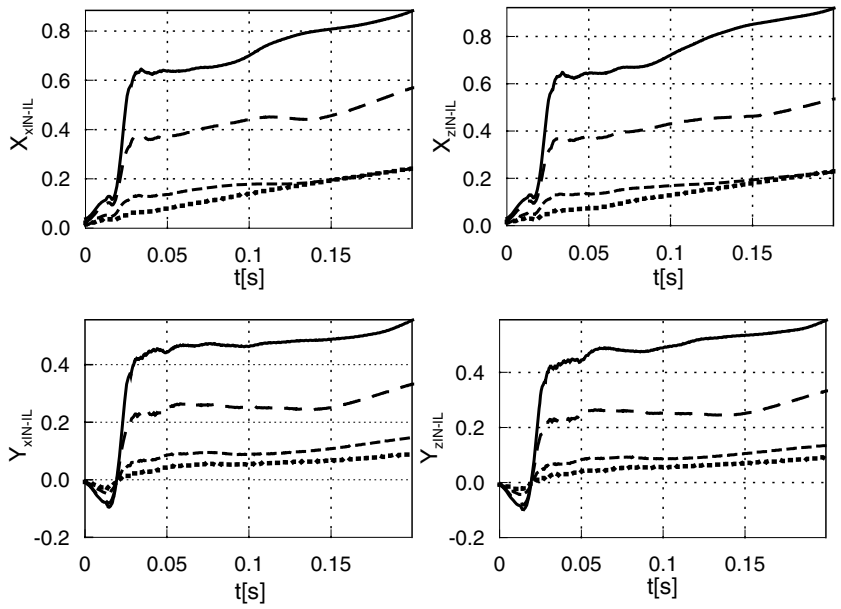

Figure 5. Time-series of X_{IN-IL} and Y_{IN-IL} under different non-linearity strengths. Solid lines: $SNp = 136.84$, $SN = 146.09$; Dashed lines: $SNp = 109.47$, $SN = 118.72$; Short Dashed lines: $SNp = 54.74$, $SN = 63.99$; Dotted lines: $SNp = 27.37$, $SN = 36.62$.

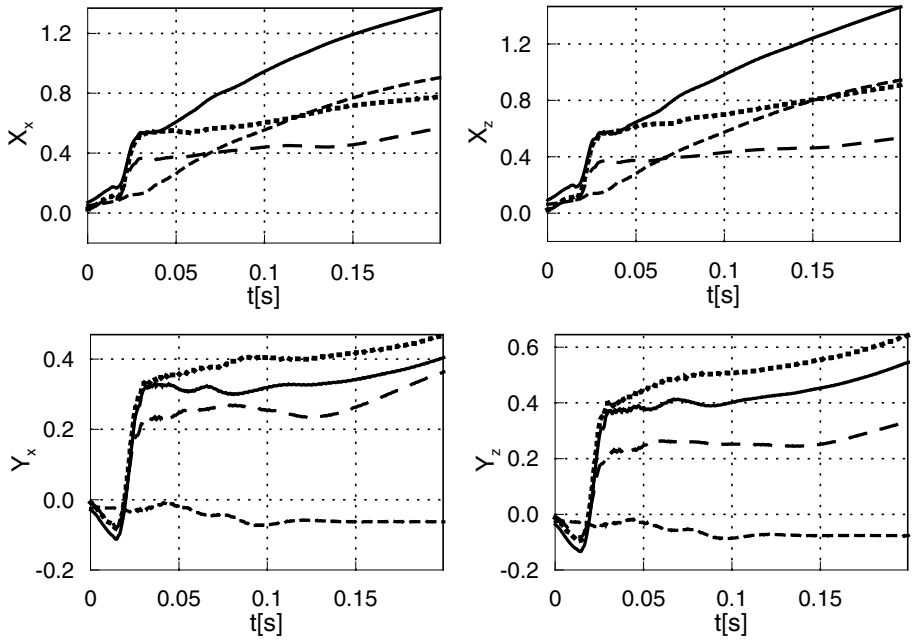

Figure 6. Four cases of X and Y time-series. Solid lines: X_{AN-IL} and Y_{AN-IL} ($SNp = 89.33$, $SN = 98.58$); Dashed lines: X_{IN-IL} and Y_{IN-IL} ($SNp = 109.47$, $SN = 118.72$); Short dashed lines: X_{AL-IL} and Y_{AL-IL}; Dotted lines: X_{AN-AL} and Y_{AN-AL} ($SNp = 93.86$, $SN = 103.00$).

a higher-order accuracy and free stable criterion to build new numerical methods and achieve more accurate solutions to non-linear elastic wave equation.

We have demonstrated clearly distinct features between the effects of anisotropy and non-linearity in this paper, although not the anisotropy but non-linearity considered in this paper is very weak compared with measured results of Rasolofosaon & Yin (1996). Particularly, the elastic wave propagation characteristics in non-linear media accumulate with traveltime and depend strongly on source energy strength. The product of source strength S_A and magnitude of non-linearity SN is the main factor dominating the non-linear characteristics of the elastic waves. Therefore, we expect that no obvious non-linear response of seismic waves may be observed when the non-linear medium is far away from the seismic source (our estimate is three to four times a wavelength) even if the strength of non-linearity of this medium may be very high. This is definitely different from the anisotropic effects, which do not depend on the medium-source distance. In this aspect, non-linear wave propagation may be considered as a 'local' and accumulated phenomenon depending strongly on source–medium distance, and the presence

© 2006 The Authors, *GJI*, **165,** 943–956
Journal compilation © 2006 RAS

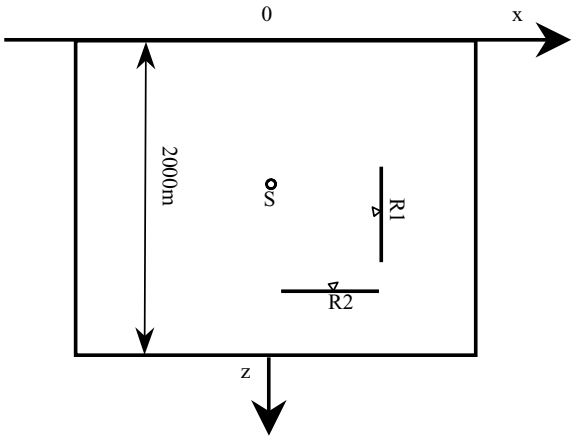

Figure 7. Structure of model 2. Seismic source is located at the centre, two receiver points $R1$ and $R2$ are located at $x = 300$ m, $z = 1160$ m and $x = 160$ m, $z = 1300$ m, respectively. The solid medium is isotropic or VTI media.

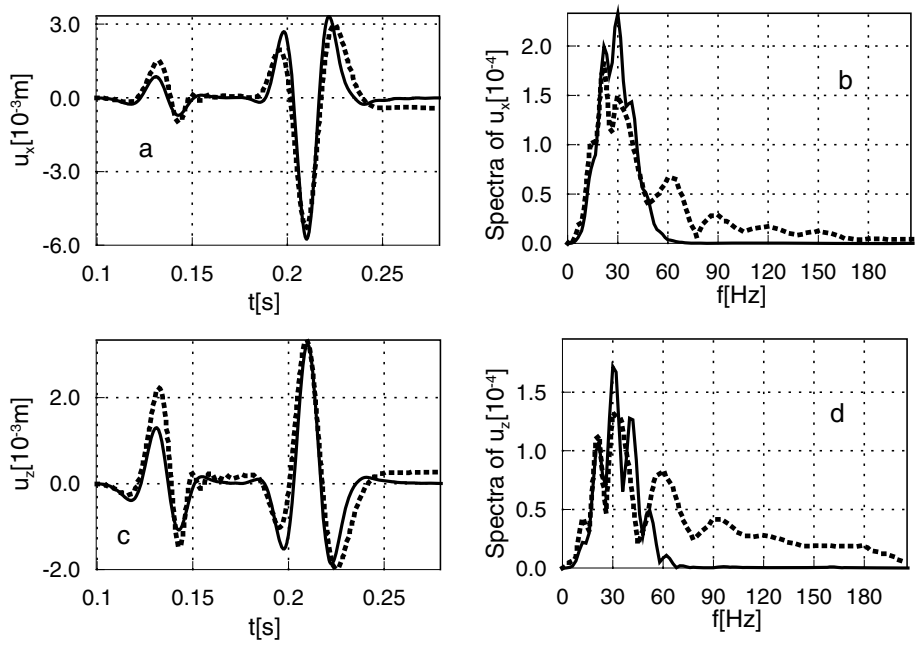

Figure 8. Linear (solid lines) and non-linear (dotted lines) waveforms and their amplitude spectra recorded at $R1$ in isotropic media ($SNp = 109.47$, $SN = 118.72$, Fig. 7). Plots a, b correspond to u_x; Plots c, d correspond to u_z.

of anisotropy can enhance the non-linear effects of wave propagation (similarly the presence of non-linearity can enhance the anisotropic effects). Note that some of the non-linear wave propagation phenomena, such as waveform distortions, resonant peak shift and harmonic generations, can easily be mistaken as due to dispersion or attenuation, and we believe that is why the non-linear effects, though observed in laboratory data repeatedly, have rarely been reported in field seismic data (while directional anisotropic effects are less likely to be mistaken).

From numerous other studies (e.g. Kazakov *et al.* 2002; Guyer & Johnson 1999), we know that different model sizes of non-linear media can display different non-linear characteristics. From our results presented in this paper, we find that non-linear responses display a more complicated relationship with model size (because of the dependence on source–medium distance) than those displayed by anisotropy (which does not really depend on source–medium distance).

ACKNOWLEDGMENTS

The work presented in this paper was supported by the National Natural Science Foundation of China (Grant Nos. 40234044, 4985108 and 40574058) and the Chinese Academy of Sciences (Grant No. KZCX2-109). We thank the Editor Dr A. J. Haines and an anonymous referee for their comments. In particular, we want to thank Professor Klaus Helbig for his very constructive comments, detailed corrections and an additional reference (Helbig 2000), which lead to the significant improvements of this paper. Enru Liu was supported by the Sponsors of Edinburgh Anisotropy Project, and this paper is published with the approval of the Executive Director of the British Geological Survey (NERC).

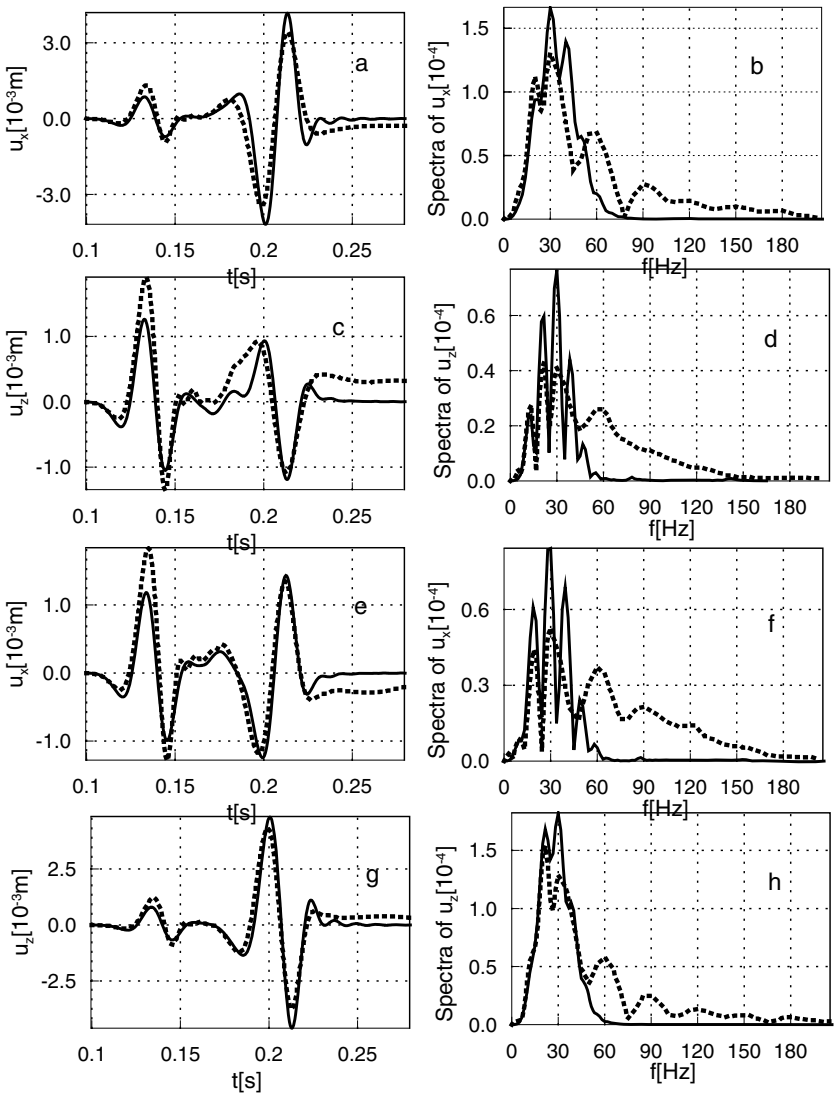

Figure 9. Linear (solid lines) and non-linear (dotted lines) waveforms and their amplitude spectra recorded at $R1$ (a, b, c, d) and $R2$ (e, f, g, h) in VTI media ($SNp = 93.86$, $SN = 103.00$, Fig. 7). Plots a, b, e, f correspond to u_x; Plots c, d, g, h correspond to u_z.

REFERENCES

Birch, F., 1961. The velocity of compressional waves in rocks to 10 kilobars, *J. geophys. Res.,* **66,** 2199–2224.

Book, D.L., Boris, J.P. & Hain, K., 1975. Flux-corrected transport II: Generalizations of the method, *J. Comput. Phys.,* **18,** 248–283.

Boris, J.P. & Book, D.L., 1973. Flux-corrected transport I: SHASTA, a fluid transport algorithm that works, *J. Comput. Phys.,* **11,** 38–69.

Boris, J.P. & Book, D.L., 1976a. Flux-corrected transport, III: minimal-error FCT algorithms, *J. Comput. Phys.,* **20,** 397–428.

Boris, J.P. & Book, D.L., 1976b. Solution of continuity equations by the method of flux-corrected transport, in *Methods of Computational Physics,* Academic Press, New York.

Bulau, J.R., Tittmann, B.R. & Abdel-Gawad, M., 1984. Nonlinear wave propagation in rock, *Proc. 1984 IEEE Ultrasonic Symposia,* 775–780.

Crampin, S., 1987. Geological and industrial applications of extensive dilatancy anisotropy, *Nature,* **328,** 491–496.

Daniel, N.O., 1997. Continuous valued cellular automata for nonlinear wave equations, *Complex Systems,* **96,** 91–119.

DeVore, C.R., 1991, Flux-corrected transport algorithms for multidimensional compressible magnetohydro-dynamics, *J. Comput. Phys.,* **92,** 142–158.

Engelbrecht, J., 1983, *Nonlinear Wave Processes of Deformation in Solids,* 1st edn, pp. 18–21, Pitman Publishing Inc, Massachusetts.

Fei, T. & Larner, K., 1995. Elimination of numerical dispersion in finite-difference modelling and migration by flux-corrected transport, *Geophysics,* **60,** 1830–1842.

Fermi, E., Pasta, J. & Ulam, S., 1974. Studies of nonlinear problems, originally in Los Alamos Report LA 1940, 1955, in S. Ulam, Sets, *Numbers and Universes,* MIT Press, Cambridge, 491–501.

Frankel, A. & Leith, W., 1992. Evaluation of topographic effects on P and S waves of explosion at the Northern Novaya Zemlya test site using 3-D numerical simulations, *Geophys. Res. Lett.,* **19,** 1887–1890.

Guyer, R.A. & Johnson, P., 1999. Nonlinear mesoscopic elasticity: evidence for a new class of materials, *Physics Today,* **52,** 30–35.

Helbig, K., 1994. *Foundations of Anisotropy for Exploration Seismics*, Handbook of Geophysical Exploration, **22,** Pergamon, Oxford.

Helbig, K., 1998. A formalism for the consistent description of non-linear elasticity of anisotropic media, *Revue de L Institut Francais du Petrole,* **53,** 693–708.

© 2006 The Authors, *GJI*, **165,** 943–956
Journal compilation © 2006 RAS

Helbig, K., 2000. Coordinate-free description of nonlinearity in anisotropic media, in *Nonlinear Acoustics at the Turn of the Millienium,* eds Lauterbom, W. & Kurz, T., eds, American Institute of Physics, Paper No. CP524 (3 pp.).

Helbig, K. & Rasolofosaon, P.N.J., 2000. A theoretical paradigm for describing hysteresis and nonlinear elasticity in arbitrary anisotropic rocks, in *Seismic Anisotropy 2000: Fractures, Converted Waves and Case Studies,* Society of Exploration Geophysicists.

Hermon, R.F.S., 1953. Third-order elastic coefficients. *Acta Cryst.,* **6,** 331–340.

Johnson, P.A. & Shankland, T.J., 1989. Nonlinear generation of elastic waves in granite and sandstone: Continuous wave and travel time observations, *J. geophys. Res.,* **94,** 17 729–17 733.

Johnson, P.A., Shankland, T.J., O'Connell, R.J. & Albright, J.N., 1987. Nonlinear generation of elastic waves in crystalline rocks, *J. geophys. Res.,* **92,** 3597–3602.

Johnson, P.A. & Rasolofosaon, P.N.J., 1996. Nonlinear elasticity and stress-induced anisotropy in rocks, *J. geophys. Res.,* **101,** 3113–3124.

Kazakov, V., Sutin, A. & Johnson, P.A., 2002. Sensitive imaging of an elastic nonlinear wave-scattering source in a solid, *Appl. Phys. Lett.,* **81,** 646–648.

Komatitsch, D. & Tromp, J., 1999. Introduction to the spectral element method for three-dimensional seismic wave propagation, *Geophys. J. Int.,* **139,** 806–822.

Kouri, D.J., Zhang, D.S. & Wei, G.W., 1999. Numerical solutions of nonlinear wave equation, *Phys. Review (E),* **59,** 1274–1277.

Landau, K.R. & Lifshitz, E.M., 1986. *Theory of Elasticity,* 3rd edn, Pergamon Press, Oxford.

Levander, A., 1988. Fourth-order finite-difference P-SV seismograms, *Geophysics,* **53,** 1425–1436.

Liu, E., Hudson, J.A. & Pointer, T., 2000. Equivalent medium representation of fractured rock, *J. geophys. Res.,* **105,** 2981–3000.

Liu, E., Queen, J.H., Li, X.Y., Chapman, M., Maultzsch, S., Lynn, H.B. & Chesnokov, E.M., 2003. Observation and analysis of frequency-dependent seismic anisotropy from a multicomponent VSP at Bluebell-Altamont Field, Utah, *J. appl. Geophys.,* **54,** 319–333.

Lynn, H., 1996. A geophysicist's view on seismic anisotropy, in *Seismic anisotropy,* pp. 1–15, eds Fjaer, E., Holt, R. & Rathore, J.S., Society of Exploration Geophysicists.

McCall, K.R., 1994. Theoretical study of nonlinear elastic propagation, *J. geophys. Res.,* **99,** 2591–2600.

McCall, K.R. & Guyer, R.A., 1994. Equation of state and wave propagation in hysteretic nonlinear elastic materials, *J. geophys. Res.,* **99,** 23887–23897.

Murnaghan, F.D., 1951. *Finite Deformation of an Elastic Solid,* 1st edn, John Wiley and Sons, Inc, New York.

Nikolaev, A.V., 1967. Seismic properties of a loose medium, *Izv. Akad. Nauk SSSR Fiz, Zemli,* **2,** 23–31.

Prosser, W.H. & Green, R.E., 1990. Characterization of the nonlinear elastic properties of Graphite/Epoxy composites using ultrasound, *J. Reinforced Plastics &Composites,* **9,** 162–173.

Prosser, W.H., Kriz, R.D. & Fitting, D.W., 1992. Nonlinear elastic effects on the energy flux deviation of ultrasonic waves in GR/EP composites, *Review of Progress in Quantitative NDE,* **11,** 2041–2048.

Rasolofosaon, P.N.J. & Yin, H., 1996. Simultaneous Characterization of anisotropy and nonlinearity in arbitrary elastic media—reflections on experimental data, in *Seismic anisotropy,* pp. 141–179, eds Fjaer, E., Holt, R. & Rathore, J.S., Society of Exploration Geophysicists.

Richtmyer, R.D. & Morton, K.W., 1967. *Difference methods for initial value problems,* Interscience, New York.

Savage, M.K., 1999. Seismic anisotropy and mantle deformation: what have we learned from shear wave splitting?, *Rev. Geophys.,* **37,** 165–206.

Scalerandi, M., Delsanto, P.P. & Chiroiu, C., 1999. Numerical simulation of pulse propagation in Nonlinear 1-D media, *J. acoust. Soc. Am.,* **106,** 2424–2430.

Schultz, C.A., 1997. A density-tapering approach for modelling the seismic response of free-surface topography, *Geophys. Res. Lett.,* **24,** 2809–2812.

Toksöz, M.N., Cheng, C.H. & Timur, A., 1976. Velocities of seismic waves in porous rocks, *Geophysics,* **41,** 621–645.

Ulam, S., 1965. *Collected Papers of Enrico Fermi,* **2,** University of Chicago Press, Chicago.

Ulam, S., 1974. Random processes and transformation, S., Ulam, *Sets, Numbers and Universes,* 326–337, MIT Press, Cambridge, MA, USA.

Vasil'ev, Yu. I., Ivanova, L.A. & Shcherbo, M.N., 1969. Measurement of stress and strain in a soil during the propagation of waves from explosions, *Izv. Akad. Nauk SSSR Fiz. Zemli,* **1,** 21–37.

Vasil'ev, Yu. I., Gvozdev, A.A., Ivanova, L.A., Molotova, L.V., Fomichev, V.B. & Shcherbo, M.N., 1977. Mechanical properties of a soft soil under stresses up to (5–10) 10^5Pa and selecting the model of the soil behaviour in strong earthquakes, in *Seismic Microzonation,* pp. 121–129, ed. Medvedev, S.V., Nauka, Moscow.

Winkler, K., Nur, A. & Gladwin, M., 1979. Friction and seismic attenuation in rocks. *Nature*, **277,** 528–531.

Xu, H., Day, S.M. & Minster, J.B.H., 1999. Two-dimensional linear and nonlinear wave propagation in a half-space, *Bull. seism. Soc. Am.,* **89,** 903–917.

Yang, D.H., Liu, E., Zhang, Z.J. & Teng, J., 2002. Finite-difference modelling in two-dimensional anisotropic media using a flux-corrected transport technique, *Geophys. J. Int.,* **148,** 320–328.

Zhang, Z.J., He, Q.D. & Teng, J., 1993. Simulation of 3-components seismic records in a 2-dimensional transversely isotropic media with finite-difference, *Can. J. Expl. Geophys.,* **29,** 51–58.

Zhang, Z.J., Wang, G.J. & Harris, J.M., 1999. Multi-component wavefield simulation in viscous extensively dilatancy anisotropic media, *Phys. Earth planet Inter.,* **114,** 25–38.

Zheng, H.S., Zhang, Z.J. & Yang, B.J., 2004. A numerical study of 1D nonlinear acoustic wave propagation in solid, *Acta Seismologica Sinica,* **17,** 80–86.

APPENDIX A: THE STABILITY CRITERION FOR THE MFCT–FD SCHEME

We consider the terms $\partial u/\partial x \approx (u^n{}_{i+1,j} - u^n{}_{i-1,j})/(2\Delta x)$ and $\partial u/\partial z \approx (u^n{}_{i,j+1} - u^n{}_{i,j-1})/(2\Delta z)$ in matrices of the **A, D, G, Q** as coefficients. According to the analyses of Richtmyer & Morton (1967) and Yang *et al.* (2002), we obtain the stability criterion for the FD scheme used in eq. (3) as follows:

$$\|\mathbf{A}\|m^2 + \|\mathbf{Q}\|k^2 \le \rho \quad \text{if} \quad \|\mathbf{D}+\mathbf{G}\| \le 2\sqrt{\|\mathbf{D}\|\cdot\|\mathbf{G}\|},$$

$$\max[F(\alpha,\beta), \|\mathbf{A}\|m^2 + \|\mathbf{Q}\|n^2] \le \rho \quad \text{if} \quad \|\mathbf{D}+\mathbf{G}\| > 2\sqrt{\|\mathbf{D}\|\cdot\|\mathbf{G}\|},$$

where

$$F(\alpha,\beta) = m^2\|\mathbf{A}\|\sin^2\alpha + n^2\|\mathbf{Q}\|\sin^2\beta + l^2\|\mathbf{D}+\mathbf{G}\|\sin 2\alpha \sin 2\beta,$$

$$\sin 2\alpha = \frac{\|\mathbf{Q}\|}{\|\mathbf{D}+\mathbf{G}\|^2}\left[\frac{\|\mathbf{D}+\mathbf{G}\|^4 - 16\|\mathbf{A}\|^2\|\mathbf{Q}\|^2}{\|\mathbf{A}\|^2/k^4 + \|\mathbf{Q}\|^2}\right]^{1/2}$$

and

$$\sin 2\beta = \frac{\|\boldsymbol{D}+\boldsymbol{G}\|\sin 2\alpha}{k\sqrt{4\|\boldsymbol{Q}\|^2 + k^2\|\boldsymbol{D}+\boldsymbol{G}\|^2\sin 2\alpha}},$$

where $k = \Delta z/\Delta x$, and $\|\cdot\|$ denotes a matrix modulus.

The items $\partial u/\partial x$ and $\partial u/\partial z$ included in each element of matrices of **A**, **D**, **G** and **Q** can be replaced by max [$abs(\partial u/\partial x)$] and max [$abs(\partial u/\partial z)$] in probing modulus of **A**, **D**, **G** and **Q**. The approximate value of max [$abs(\partial u/\partial x)$] and max [$abs(\partial u/\partial z)$] can be reported by the numerical test of small size regions.

APPENDIX B: THE MODIFIED CENTRAL FINITE DIFFERENCE FCT ALGORITHM

This MFCT algorithm presented in this paper consists of the following steps:

1. Application of finite-difference scheme to eq. (3) to compute $u_{i,j}^{n+1}$ where $n \geq 0$.
2. Numerically corrected solution. The modified solution is

$$\tilde{u}^{n+1} = \text{limiter}\left(u_{i,j}^{n+1}\right) = \text{sign}\left(u_{i,j}^{n+1}\right)\cdot\min[abs\left(u_{i,j}^{n+1}\right), u_a, u_b], \tag{B1}$$

where $u_a = f[abs(u_{i,j}^{n+1}) - a_1\, s] + a_1\, s$, $u_b = a_2\, s$, $a_2 > a_1 > 0$, and can be taken as constants; $f(x) > 0$ if $x > 0$ and satisfies $f(x_1) > f(x_2) > 0$ if $x_1 > x_2 > 0$, $f(x) = 0$ if $x \leq 0$; $s > 0$ is a constant depending on the power of the source.

3. Diffusion computation. We distinguish two steps:

3.1 Computing diffusive fluxes at the nth time step:

$$p_{i+1/2,j}^{n} = \sigma_1\left[\left(\tilde{u}_{i+1,j}^{n} - \tilde{u}_{i,j}^{n}\right) - \left(\tilde{u}_{i+1,j}^{n-1} - \tilde{u}_{i,j}^{n-1}\right)\right],$$

$$q_{i,j+1/2}^{n} = \sigma_1\left[\left(\tilde{u}_{i,j+1}^{n} - \tilde{u}_{i,j}^{n}\right) - \left(\tilde{u}_{i,j+1}^{n-1} - \tilde{u}_{i,j}^{n-1}\right)\right],$$

where $\sigma_1 (0 \leq \sigma_1 \leq 1)$ is the smoothing parameter for displacement u_i. Usually, it can be chosen as a constant determined from a few small-scale numerical experiments. In this paper, we find $0.005 \leq \sigma_1 \leq 0.095$ is acceptable for our numerical examples.

3.2 Smoothing the corrected solution of eq. (3), $\tilde{u}^{n+1}$, through diffusive fluxes p and q:

$$\overline{u}_{i,j}^{n+1} = \tilde{u}^{n+1} + \left(p_{i+1/2,j}^{n} - p_{i-1/2,j}^{n}\right) + \left(q_{i,j+1/2}^{n} - q_{i,j-1/2}^{n}\right). \tag{B2}$$

4. Offsetting diffusion. Here we distinguish three steps:

4.1 Computing diffusive fluxes at the $n+1$ time step:

$$\overline{p}_{i+1/2,j}^{n+1} = \sigma_2\left[\left(\tilde{u}_{i+1,j}^{n+1} - \tilde{u}_{i,j}^{n+1}\right) - \left(\tilde{u}_{i+1,j}^{n} - \tilde{u}_{i,j}^{n}\right)\right],$$

$$\overline{q}_{i,j+1/2}^{n+!} = \sigma_2\left[\left(\tilde{u}_{i,j+1}^{n+1} - \tilde{u}_{i,j}^{n+!}\right) - \left(\tilde{u}_{i,j+1}^{n} - \tilde{u}_{i,j}^{n}\right)\right],$$

where $\sigma_2 (0 \leq \sigma_2 \leq 1)$ is the compensation parameter for displacement or amplitude. In this paper, σ_2 is chosen as a constant and taken as about 5–15 per cent larger than σ_1.

4.2 Utilizing the modified and the corrected solutions to compute the offsetting diffusive fluxes:

$$x_{i+1/2,j} = \left(\overline{u}_{i+1,j}^{n+1} - \overline{u}_{i,j}^{n+1}\right) - \left(\tilde{u}_{i+1,j}^{n} - \tilde{u}_{i,j}^{n}\right),$$

$$z_{i,j+1/2} = \left(\overline{u}_{i,j+1}^{n+1} - \overline{u}_{i,j}^{n+!}\right) - \left(\tilde{u}_{i,j+1}^{n} - \tilde{u}_{i,j}^{n}\right).$$

4.3 Utilizing the offsetting diffusive fluxes and modifying the solution $\bar{u}_{i,j}^{n+1}$ again, then we finally obtain the corrected solution

$$u_{i,j}^{n+1} = \overline{u}_{i,j}^{n+1} - \left(\overline{x}_{i+1/2,j} - \overline{x}_{i-1/2,j}\right) - \left(\overline{z}_{i,j+1/2} - \overline{z}_{i,j-1/2}\right), \tag{B3}$$

where

$$\overline{x}_{i+1/2,j} = s^x \cdot \max\left\{0, \min\left[s^x \cdot x_{i-1/2,j}, abs\left(\overline{p}_{i+1/2,j}^{n+1}\right), s^x \cdot x_{i+3/2,j}\right]\right\},$$

$$\overline{z}_{i,j+1/2} = s^z \cdot \max\left\{0, \min\left[s^z \cdot z_{i,j-1/2}, abs\left(\overline{q}_{i,j+1/2}^{n+1}\right), s^z \cdot z_{i,j+3/2}\right]\right\},$$

$$s^x = \text{sign}\left(\overline{p}_{i+1/2,j}^{n+1}\right), s^z = sign\left(\overline{q}_{i,j+1/2}^{n+1}\right).$$

We perform the numerical calculation by repeating stages $1 \sim 4$.

APPENDIX C: THE NORMS OF SOE AND TOE VECTORS

To represent the global non-linearity in 3-D media, the explicit expressions of the norms $\tilde{C}^{\text{Linear}}$, $\tilde{C}^{\text{NLphysical}}$ and $\tilde{C}^{\text{NLgeometrical}}$ are given below. To study the differences between the SOE and TOE coefficients, the absolute value of each elastic constant is used. Note that we use the sum of absolute values to give a rough estimate of the strength of non-linearity only and it would be more proper to use the sum of the squared

© 2006 The Authors, *GJI*, **165,** 943–956
Journal compilation © 2006 RAS

values (or Euclidean norm) or coordinate-free representation of elastic tensors as pointed by one of the reviewers Professor K. Helbig in his paper (Helbig 2000). The norm of the linear elastic coefficients is

$$\begin{aligned}\|\tilde{C}^{\text{Linear}}\| = {} & |C_{11}| + 2|C_{12}| + 2|C_{13}| + 4|C_{14}| + 4|C_{15}| + 4|C_{16}| + |C_{22}| \\ & + 2|C_{23}| + 4|C_{24}| + 4|C_{25}| + 4|C_{26}| + |C_{33}| + 4|C_{34}| + 4|C_{35}| \\ & + 4|C_{36}| + 4|C_{44}| + 8|C_{45}| + 8|C_{46}| + 4|C_{55}| + 8|C_{56}| + 4|C_{66}|. \end{aligned} \tag{C1}$$

The norm of the physical non-linear elastic coefficients is

$$\begin{aligned}\|\tilde{C}^{\text{NLphysical}}\| = {} & |C_{111}| + 3\,|C_{112}| + 3\,|C_{113}| + 6\,|C_{114}| + 6\,|C_{115}| + 6\,|C_{116}| + 3\,|C_{122}| + 6\,|C_{123}| \\ & + 12\,|C_{124}| + 12\,|C_{125}| + 12\,|C_{126}| + 3\,|C_{133}| + 12\,|C_{134}| + 12\,|C_{135}| + 12\,|C_{136}| \\ & + 12\,|C_{144}| + 24\,|C_{145}| + 24\,|C_{146}| + +12\,|C_{155}| + 24\,|C_{156}| + 12\,|C_{166}| + |C_{222}| \\ & + 3\,|C_{223}| + 6\,|C_{224}| + 6\,|C_{225}| + 6\,|C_{226}| + 3\,|C_{233}| + 12\,|C_{234}| + 12\,|C_{235}| \\ & + 12\,|C_{236}| + 12\,|C_{244}| + 24\,|C_{245}| + 24\,|C_{246}| + 12\,|C_{255}| + 24\,|C_{256}| + 12\,|C_{266}| \\ & + |C_{333}| + 6\,|C_{334}| + 6\,|C_{335}| + 6\,|C_{336}| + 12\,|C_{344}| + 24\,|C_{345}| + 24\,|C_{346}| \\ & + 12\,|C_{355}| + 24\,|C_{356}| + 12\,|C_{366}| + 8\,|C_{444}| + 24\,|C_{445}| + 24\,|C_{446}| + 24\,|C_{455}| \\ & + 48\,|C_{456}| + 24\,|C_{466}| + 8\,|C_{555}| + 24\,|C_{556}| + 24\,|C_{566}| + 8\,|C_{666}|\,. \end{aligned} \tag{C2}$$

The norm of the geometrical non-linear elastic tensor is

$$\begin{aligned}\|\tilde{C}^{\text{NLgeometrical}}\| = {} & 15|C_{11}| + 12|C_{12}| + 12|C_{13}| + 24|C_{14}| + 60|C_{15}| + 60|C_{16}| \\ & + 15|C_{22}| + 12|C_{23}| + 60|C_{24}| + 24|C_{25}| + 60|C_{26}| + 15|C_{33}| \\ & + 60|C_{34}| + 60|C_{35}| + 24|C_{36}| + 42|C_{44}| + 84|C_{45}| + 84|C_{46}| \\ & + 42|C_{55}| + 84|C_{56}| + 42|C_{66}| + 2\,|2C_{36} + C_{45}| + 4\,|C_{36} + 4C_{45}| \\ & + 4\,|2C_{25} + C_{46}| + 4\,|C_{25} + 2C_{46}| + 2\,|2C_{13} + C_{55}| + 2\,|C_{13} + 2C_{55}| \\ & + 4\,|2C_{14} + C_{56}| + 4\,|C_{14} + 2C_{56}| + 2\,|2C_{12} + C_{66}| + 2\,|C_{12} + 2C_{66}|\,. \end{aligned} \tag{C3}$$

Only the values of C_{11}, C_{13}, C_{33}, C_{55}, C_{111}, C_{113}, C_{133}, C_{155} and $C_{355}$are needed for a VTI medium; the other elastic tensors in eqs (C1), (C2) and (C3) are set equal to zero when we calculate SN_p, SN_g and SN given in eq. (5).

© 2006 The Authors, *GJI*, **165,** 943–956
Journal compilation © 2006 RAS